International Journal of Modern Physics A

Realizing laminar-like flow in charged bunches with density evolution equations

B. S. Zerbe

Department of Physics and Astronomy,
Michigan State University, [48224] East Lansing, MI USA
zerbe@pa.msu.edu

P. M. Duxbury

Department of Physics and Astronomy,
Michigan State University, [48224] East Lansing, MI USA
duxbury@pa.msu.edu

Received Day Month Year
Revised Day Month Year

In the ultra-fast electron microscopy community, electron bunches with much smaller longitudinal widths than transverse widths are emitted from the cathode surface. The community has believed that these bunches evolve to a uniform ellipsoid, but recent simulations by our group and others suggest that if the bunch has an initially transverse Gaussian profile, a ring-like density "shock" emerges at the median of the bunch during evolution. To explain these results, we generalized Reed's 1D fluid model of charged bunch expansion to cylindrical and spherical geometries demonstrating such a shock emerges analytically under these symmetric geometries. Mathematically, the shock in these models occurs when particles more toward the middle "catch-up" to outer particles, and eventually the trajectory of the more central particle crosses-over the outer particle's trajectory. This crossover marks the transition from the laminar to non-laminar regime. However, this theory has been developed for cold-bunches, i.e. bunches of electrons with zero initial momentum. Here, we briefly review this new theory and extend it to the cylindrically- and spherically- symmetric cases that have non-zero initial momentum. This formulation elucidates how charge-dominated bunches may be manipulated to maintain laminar conditions even through focussing of the bunch.

Keywords: density evolution equations; non-neutral plasma; coulomb explosion; laminar

PACS numbers:47.15.-x 47.15.Tr 47.27.C 41.20.-q 41.75.-i 42.65.Jx 45.05.+x

1. Introduction

Freely expanding ensembles of charged particles are fundamental to accelerator physics. Although continuous beams near the particle source are relatively diffuse, bunched beams can reach densities where space-charge effects dominate the expansion. A seminal work by Luiten et.[1] reasoned that pancake bunches under such space-charge dominated expansion should become uniform ellipsoids if they had the correct initial, non-uniform distribution based on essentially complementary work

that had been done on the collapse of a uniform ellipsoid under gravity in astrophysics.[2] This postulate has been supported by experimental evidence that observed the uniform-like projected density of an ellipsoid after such expansion.[3] However, we recently published simulated results that showed that initially Gaussian transverse distributions in this pancake regime may appear uniform when projected, but the evolved distribution actually obtains a ring-like substructure around the median of the beam.[4]

A number of theoretical approaches have been used to understand beam dynamics that could arguably shed light on this density ring. More than 30 years ago, Anderson presented 1D and cylindrical mean-field fluid models of beam dynamics for ensembles of particles with arbitrary initial distributions relevant while the beam remains laminar.[5] These models describe the transverse density in the presence of a focussing force — a model that eventually helped lead to emittance compensation.[6,7] However, these models are for cigar-like beams and not pancake-like bunches and are therefore inappropriate. Within the ultrafast electron microscopy (UEM) literature, numerous works postulated 1D models for non-relativistic longitudinal free expansion,[1,8,9] and Reed eventually settled upon a mean-field fluid approach. Again this model was to describe the longitudinal density evolution of initially dense pancake bunches that can be assumed to be planar symmetric. Reed's mean-field model accurately describes the longitudinal expansion while planar symmetry can be assumed.[10] However, Reed was concerned that no Coulomb explosion-like shock was seen in the model even when non-uniform initial conditions were assumed, in stark disagreement to what had been previously found within the Coulomb explosion literature.[11–16] We recently demonstrated that such a shock cannot occur in the non-relativistic 1D model without careful tuning of the initial velocity distribution.[4] In contrast, we showed that these shocks spontaneously occur in higher dimensions for non-uniform distributions,[4] so that the theoretical results found in the UEM community are now consistent with the shocks found in the Coulomb explosion literature as well as observed in our simulations of the evolution of a pancake bunch.

We accomplished this demonstration by generalizing Reed's model to higher dimension by deriving closed form analytic expressions that describe arbitrary density evolution under cylindrical and spherical symmetries with cold initial conditions, meaning that all particles are assumed to start with 0 velocity.[4] We recently discovered a paper from the Coulomb explosion literature that has the same spherically symmetric analysis we presented in our work but pre-dates our publication by roughly a decade;[17] however, we presented not only the spherically symmetric analysis but the planar and cylindrically symmetric analyses as well. We found that the shocks arise when the Lagrangian particles from our model approach one another. Eventually, Lagrangian particles in these shocks will cross, which in essence is a violation of laminar conditions – an assumption of the analysis; while the model still approximates the simulations after such a cross-over event in the free expansion case, this is due to the dynamics being largely determined by the early evolution

of the bunch where the space-charge forces are strongest. On the other hand, if the laminar assumption is violated in a region where space-charge forces dominate, we would expect the model to differ from the simulation. Therefore, we argue that our equations and the simulation deviations from the model's predictions may be used as a proxy for understanding laminar conditions in the presence of the non-linear forces typical of dense bunches at cross-over.

This is significant to the community as laminar-like flow in a charged particle beam produces ideal conditions for experiments;[18] specifically, it is important to understand to what extent space-charge dominated bunches can be manipulated to maintain laminar-like conditions. However, our previous model assumes that the initial velocity of every particle is 0. Here we present an extension of our previous model that includes arbitrary initial velocities that can be written as a single-value function of the radius of the appropriate symmetry, i.e. $v_0 = v_0(r_0)$. This is still a cold distribution as it has no initial emittance, but it can now be used to treat driven expansion and focussing events by specifying the form of $f(r_0)$. We demonstrate that this model reproduces particle-in-cell (PIC) simulations, implemented in warp[19] for many cases. We also validate our spherically symmetric results using N-particle simulations implemented in Fortran using the fast multipole method (FMM) library, fmm3dlib.[20] We show conditions where the laminar assumption is violated and obtain analytical bounds for when the laminar assumption can be maintained through focal points for arbitrary distributions within the space-charge dominated regime.

2. Density evolution with initial velocity

In this section, we present a derivation of the density evolution equations with arbitrary initial velocity, $\vec{v}_0 = v_0(r)\hat{r}$, under cylindrical and spherical symmetries. This analysis follows from our earlier work[4] with the following differences: (1.) we assume non-zero radial velocity and (2.) we adopt slightly modified notation that we have recently developed for a relativistic extension of our initial analysis (under review).

Consider Lagrangian particles under cylindrical and spherical symmetries. Let the position of the particles be parameterized by $r = \sqrt{x^2 + y^2}$ in the cylindrical case and $r = \sqrt{x^2 + y^2 + z^2}$ in the spherical case. Further, denote V_d for $d \in \{2, 3\}$ as the Jacobian of the transformation from the specific symmetry to a $1D$ formulation, namely $V_2 = 2\pi r$, and $V_3 = 4\pi r^2$. Furthermore, introduce the subscript 0 to indicate the initial (at time 0) value of any parameter; for example, r_0 indicates the initial position of a Langragian particle under the model. Likewise, denote $V_{0d} = V_d(r_0)$, i.e. $V_{02} = 2\pi r_0$, and $V_{03} = 4\pi r_0^2$.

Consider an ensemble of particles. Define the time-dependent probability density (fraction of entire distribution per unit area), $\rho_d(r; t)$, and denote the initial probability density as $\rho_{0d} = \rho_{0d}(r_0) = \rho_d(r_0; t = 0)$. With the initial conditions, we

have,

$$P_{0d} = \int_0^{r_0} V_{0d}\rho_{0d}(r)dr \tag{1}$$

$$E_{0d}(r_0) = E_{0d} = \frac{Q_{tot,d}P_{0d}}{V_{0d}\epsilon_0} \tag{2}$$

where $Q_{tot,d}$ is the total charge per unit length along the cylindrical charge distribution under cylindrical symmetry or the total charge under spherical symmetry and P_{0d} is the cumulative probability within r_0. Notice that the quantity $Q_{tot,d}P_{0d}$ represents the charge per unit length or charge inside radius r_0 for the cylindrically and spherically symmetric cases, respectively. As P_{0d} is the cumulative probability contained in r_0 and $\int_0^{r_0} V_d(r)dr$ is the volume contained in r_0, the average probability density can be defined by

$$\bar{\rho}_{0d} = \frac{P_{0d}}{\int_0^{r_0} V_d(r)dr} \tag{3}$$

Assuming the distribution undergoes laminar flow, the electric field experienced by a particle at radial position $r(r_0, t)$ under cylindrical ($d = 2$) and spherical ($d = 3$) symmetries, respectively, is

$$E_d(r) = E_{0d}\left(\frac{r_0}{r}\right)^{d-1} \tag{4}$$

Under the laminar assumption, E_{0d} is a constant, and the change in kinetic energy is found by integrating the force qE:

$$\Delta K_2 = \mathcal{E}_{r2}\ln\left(\frac{r}{r_0}\right) \tag{5}$$

$$\Delta K_3 = \mathcal{E}_{r3}\left(1 - \frac{r_0}{r}\right) \tag{6}$$

for the cylindrical and spherical cases, respectively. Here $\mathcal{E}_{rd} = \frac{qQ_{tot,d}P_{0d}r_0}{V_{0,d}\epsilon_0}$. Further introduce a fictitious velocity, v_{rd} for $d = 2, 3$, such that $v_{rd} = +\sqrt{\frac{2\mathcal{E}_{rd}}{m}}$. Using conservation of energy in the non-relativistic regime with initial energy $\mathcal{E}_0 = \frac{1}{2}mv_0^2$, we can solve for the velocity,

$$\frac{v_2}{v_{r2}} = \pm\sqrt{\frac{\mathcal{E}_0}{\mathcal{E}_{r2}} + \ln\left(\frac{r}{r_0}\right)}$$

$$\frac{v_3}{v_{r3}} = \pm\sqrt{\frac{\mathcal{E}_0}{\mathcal{E}_{r3}} + 1 - \frac{r_0}{r}}$$

where the $\pm$ is determined by whether the particle is traveling away or toward the origin and the subscript again indicates the appropriate symmetry. In other words, the velocity equations become double valued for $r < r_0$ when $v_0 < 0$ as both the negative and positive square roots occur at some time $t > 0$; specifically, there is a radius, $r_{td} < r_0$ with $d = 2, 3$, at which the Lagrangian particle reaches 0 velocity and turns-around, and the velocities between this r_{td} and r_0 are symmetric

— differing only by their sign. The geometric interpretation of this radius can be seen in Fig. 1. By setting $v = 0$, r_{td} can be derived

$$r_{t2} = r_0 e^{-\frac{v_0^2}{v_{r2}^2}} \tag{7}$$

$$r_{t3} = \frac{r_0}{1 + \frac{v_0^2}{v_{r3}^2}} \tag{8}$$

With this notation, the velocities can be rewritten as

$$\frac{v_2}{v_{t2}} = \pm\sqrt{\ln\left(\frac{r}{r_{t2}}\right)} \tag{9}$$

$$\frac{v_3}{v_{t3}} = \pm\sqrt{1 - \frac{r_{t3}}{r}} \tag{10}$$

where $v_{t2} = \sqrt{\frac{qQ_{tot,2}P_{02}}{\pi m\epsilon_0}} = v_{r2}$ and $v_{t3} = \sqrt{\frac{qQ_{tot,3}P_{03}}{2\pi m\epsilon_0 r_{t3}}} = v_{r3}\sqrt{\frac{r_0}{r_{t3}}}$. We use these turn-around radii to define the average probability-like densities

$$\bar{\rho}_{t2} = \frac{P_{02}}{\pi r_{t2}^2} \tag{11}$$

$$\bar{\rho}_{t3} = \frac{P_{03}}{\frac{4}{3}\pi r_{t3}^3} \tag{12}$$

and the associated plasma frequencies

$$\omega_{t2} = \sqrt{\frac{qQ_{tot,2}\bar{\rho}_{t2}}{\epsilon_0 m}} = \frac{v_{t2}}{r_{t2}} \tag{13}$$

$$\omega_{t3} = \sqrt{\frac{2}{3}}\sqrt{\frac{qQ_{tot,3}\bar{\rho}_{t3}}{\epsilon_0 m}} = \frac{v_{t3}}{r_{t3}} \tag{14}$$

thus effectively mapping this problem to the freely-expanding case started from rest we recently examined.[4] The main difference, now, is that r_{td} and ω_{td} are functions of both r_0 and v_0 whereas in the from rest theory their counterparts, r_0 and ω_{p0d}, were treated as functions solely of r_0. Furthermore, r_{td} does not necessary occur at the same time for all Lagrangian particles. That is, as the bunch contracts, different portions of the bunch can reverse their course and begin to expand locally — the entire bunch need not enter into the expansion regime at the same time. This is in contrast to our earlier solution where the bunch began expansion at the same time; however, it should be noted that the mathematics for these cases is extremely similar. Of course, this difference in expansion time will complicate the derivation of r' where $' \equiv \frac{d}{dr_0}$, but it will much simplify the derivation and interpretation of the time-position relation.

To derive the time-position relation for a specific Lagrangian particle, we consider the normal time-position relation with r_0 replaced by r_{td}. If $v_0 > 0$, then the time-position relation is the same as the cold expansion relations less the time it would take the particle to travel from r_{td} to r_0, call this t_d for $d = 2, 3$. If $v_0 < 0$, then the particle needs to travel from r_0 to r_{td} before undergoing free expansion

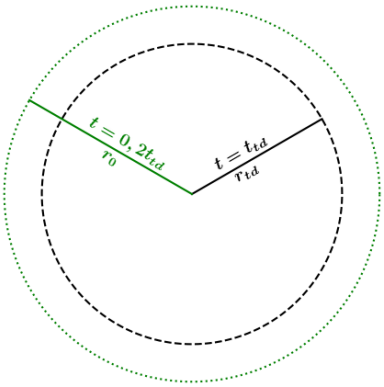

Fig. 1. Schematic detailing meaning of different radii for a single Lagrangian particle at different times represented here by concentric circles. The particle starts at r_0 at $t = 0$ represented by the green (online) dotted circle with velocity v_0. According to the laminar assumption, the velocity of the particle at every radius can be calculated by conservation of energy, and the black (online) dashed circle with radius r_{td}, always closer to the origin than r_0, denotes the radius where the velocity is 0. The corresponding time at which the particle is at r_{td} is denoted t_{td}; $t_{td} < 0$ if $v_0 > 0$ and $t_{td} > 0$ if $v_0 < 0$. We previously solved the evolution of the Lagrangian particle from rest,[4] and the non-rest evolution can be expressed in terms of the solution starting from r_{td} at t_{td}. Notice that according to the symmetry of this problem, the particle returns to r_0 at $2t_{td}$ with velocity $-v_0$.

expansion from rest. As this process is symmetric to the expansion from r_{td} to r_0, the alteration is again t_{td}. Denote t_{ftd} as the portion of the time-position relation defined by the cold free-expansion from r_{td}. Thus, $t = \pm t_{ftd} - t_{td}$ where the $\pm$ sign is determined by whether the Lagrangian particle is moving away or toward the origin, respectively, t_d has the same sign as v_0, and $d = 2, 3$ for the cylindrical and spherical symmetric case, respectively. The parameter t_{ftd} can be determined from our previous work:[4]

$$t_{ft2} = \frac{2}{\omega_{t2}} e^{y_2^2} F(y_2) \tag{15}$$

$$t_{ft3} = \frac{1}{\omega_{t3}} \left(\tanh^{-1} y_3 + \frac{y_3}{1 - y_3^2} \right) \tag{16}$$

where $y_2 = \sqrt{\ln\left(\frac{r}{r_{t2}}\right)}$, $y_3 = \sqrt{1 - \frac{r_{t3}}{r}}$, and $F(\cdot)$ represents the Dawson function. From these equations, we can also obtain t_{td}

$$t_{t2} = \frac{2}{\omega_{t2}} e^{\frac{v_0^2}{v_{r2}^2}} F\left(\frac{v_0}{v_{r2}}\right) \tag{17}$$

$$t_{t3} = \frac{1}{\omega_{t3}} \left(\tanh^{-1}\left(\frac{v_0}{\sqrt{v_0^2 + v_{r3}^2}}\right) + \frac{v_0\sqrt{v_0^2 + v_{r3}^2}}{v_{r3}^2} \right) \tag{18}$$

Implicit differentiation of t allows us to determine $r' = \frac{dr}{dr_0}$ which is used in the

density evolution expression

$$\rho_d(r;t) = \frac{\rho_{0d}}{\left(\frac{r}{r_0}\right)^{d-1} r'} \tag{19}$$

To obtain an expression for r', we need to take the derivative of the time with respect to r_0 while holding t constant, and then we solve for r'. We present the results of this process written in terms of time, the ratio $\frac{r}{r_{td}}$, and the initial conditions

$$r' = \begin{cases} -y_d r_{td}\omega_{td} t'_{td} + y_d r_{td}\omega'_{td} t_{ftd} + \frac{r}{r_{td}} r'_{td}, & t < -t_{td} \\ y_d r_{td}\omega_{td} t'_{td} + y_d r_{td}\omega'_{td} t_{ftd} + \frac{r}{r_{td}} r'_{td}, & t \geq -t_{td} \end{cases} \tag{20}$$

for $d = 2, 3$ for the cylindrical and spherical symmetric case, respectively. Note that the condition on the time corresponds to the same $\pm$ condition seen with the velocity and the time-position relation. Further notice that all of the derivatives on the right hand side can be written in terms of r_0, v_0, v'_0, and ρ_{0d}; namely

$$r'_{td} = \frac{r_{td}^{d-1}}{r_0^{d-1}} \left(1 - 2\frac{v_0}{v_{rd}}\frac{r_0 v'_0}{v_{rd}} + d\frac{v_0^2}{v_{rd}^2}\frac{\rho_{0d}}{\bar{\rho}_{0d}}\right) \tag{21}$$

$$\omega'_{td} = \frac{d}{2}\frac{\omega_{td}}{r_0}\left(\frac{\rho_{0d}}{\bar{\rho}_{0d}} - \frac{r_0}{r_{td}} r'_{td}\right) \tag{22}$$

$$t'_{t2} = -\frac{t_{t2}}{\omega_{t2}}\omega'_{t2} + \frac{2}{\omega_{t2}}\frac{v_0}{v_{r2}} e^{\frac{v_0^2}{v_{r2}^2}} \frac{1}{r_0}\left(\frac{r_0 v'_0}{v_0} - \frac{\rho_{02}}{\bar{\rho}_{02}}\right) \tag{23}$$

$$t'_{t3} = -\frac{t_{t3}}{\omega_{t3}}\omega'_{t3} + \frac{1}{\omega_{t3}}\frac{v_0}{v_{r3}}\sqrt{1 + \frac{v_0^2}{v_{r3}^2}}\frac{1}{r_0}\left(1 + 2\frac{r_0 v'_0}{v_0} - 3\frac{\rho_{03}}{\bar{\rho}_{03}}\right) \tag{24}$$

We present the derivation of Eqs. (21) - (24) in Appendix A. Eq. (20) leads to an analytic form for $\rho_d(r;t)$ once it is applied to Eq. (19).

3. Comparison to cylindrically-symmetric simulations

We first demonstrate the use of these equation with initially uniform distributions under cylindrical symmetry. Within the initial distribution, we introduce a velocity term that is linear in the initial position, specifically it has the form $v_0(r_0) = C\frac{r_0}{R}$ where C is a simulation dependent constant and R is the initial radius of the uniform distribution. This form for the velocity was chosen as it models the linear kick received by a distribution as it passes through a typical focussing lens. For our demonstration, we chose $Q_{tot,2} = 2 \times 10^7 \frac{e}{m}$ and $R = 1mm$, and this corresponds to a $v_{r2} \approx 10^5 \frac{m}{s}\frac{r_0}{R}$. For the purposes of simulation, we used the electrostatic Poisson solver in warp.[19] Fig. 2 shows the results for one value for $C = -10^5 m/s$, which is nearly equal to the constant associated with v_{r2}. As can be seen, the theory is in excellent agreement even through the focal point of the distribution. We have examined other values for C, and such agreement is generally witnessed. We point out that this agreement is in part due to both the initial velocity and v_{r2} having the same functional form, $\frac{r_0}{R}$, thus the distribution remains laminar.

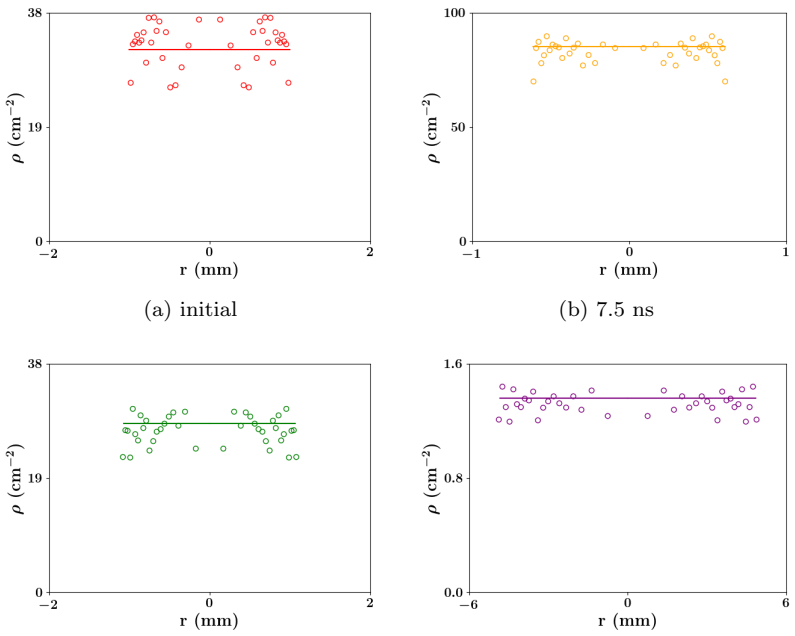

(a) initial (b) 7.5 ns

(c) 15 ns (d) 37.5 ns

Fig. 2. The evolution of cylindrically symmetric uniformly distributed electrons with density of $2 \times 10^7 \frac{e}{m}$ in a $R = 1$ mm radius with initial velocity assigned by $v_0 = -100 \frac{r_0}{R} \frac{km}{s}$, where r_0 represent the radial position of the particle, at t is (a) 0, (b) 7.5 ns, (c) 15 ns, and (d) 37.5 ns. Solid lines are from the theory presented in this paper and circles are from the same single PIC simulation but at the different times. Note the different scales on the axes for the different plots except (a) and (c), and further note that the model captures both the contraction as well as the expansion of the bunch. Specifically, note that (a) and (c) are nearly the same distribution as here t_{2d} is slightly less than 7.5 ns.

We next demonstrate the use of these equations with initially Gaussian distributions under cylindrical symmetry. Again we introduce the same initial velocity relation, $v_0(r_0) = C\frac{r_0}{R}$, choosing $Q_{tot,2} = 4 \times 10^7 \frac{e}{m}$ and $\sigma_r = 1mm$, which corresponds to a $v_{r2} \approx 1.4 \times 10^5 \frac{m}{s} \sqrt{1 - e^{-\frac{r_0^2}{2\sigma_r^2}}}$. Unlike the uniform case, the functional form for the initial velocity and the velocity scale differ. As we are interested in when the laminar assumption fails, we examine multiple values of C. Figs. 3 and 4 show the evolution for the two positive values of C less than and near the value of v_{r2}. For all such cases examined, the theory and the simulations were again in excellent agreement. For $C = 10^4 \frac{m}{s}$, we see that the shock emerges approximately at 22 ns instead of the 20 ns emergence seen in the cold case.[4] For $C = 5 \times 10^4 \frac{m}{s}$, the shock is far less noticeable and emerges in the vicinity of $50ns$. For $C = 10^5 \frac{m}{s}$ (not shown), the distribution become much closer to the uniform distribution and we could not see the emergence of the shock even at times $> 100ns$. This suggests that the violation of the laminar condition that occurs shortly after the formation of

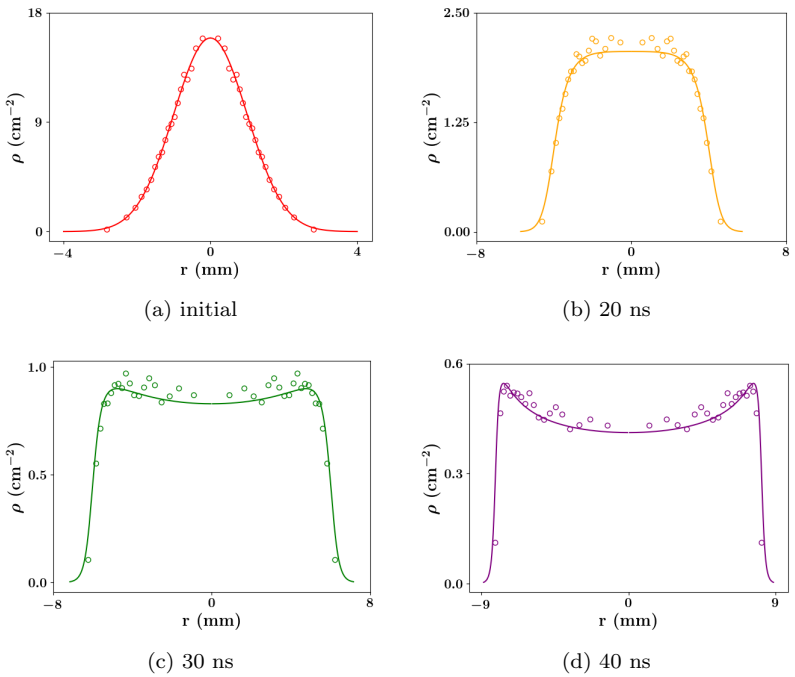

(a) initial (b) 20 ns

(c) 30 ns (d) 40 ns

Fig. 3. Similar to Fig. 2 but with $v_0 = 10\frac{r_0}{R}\frac{km}{s}$, with the initial Gaussian distribution, and where t is (a) 0, (b) 20 ns, (c) 30 ns, and (d) 40 ns. Solid lines are from the theory presented in this paper and circles are from the same single PIC simulation but at the different times; note the different scales on the axes for the different plots. Further note that the model captures the emergence of the density peak between 20 ns and 30 ns, aka shock in the Coulomb explosion literature, and is very apparent by (d) 40 ns. The emergence of this shock is slightly delayed from what we found in the initially at rest case.[4]

the shock can be delayed by putting a large, linear outward initial velocity relation on the bunch.

Figs. 5, 6, and 7 show the evolution for the three negative values of C. We see that for $C = -10^4\frac{m}{s}$ the shock emerges around 18 ns instead of the 20 ns emergence seen in the cold case, and for $C = -5 \times 10^4\frac{m}{s}$ the shock seems to emerge in the vicinity of 11 ns. However, the deviation of the simulated density from the theoretical expectation is much larger for this simulation than for the previously investigated simulations indicating that the model assumption may be only approximate. Interestingly, the model predicts qualitatively different behavior than what is seen in simulation for $C = -10^5\frac{m}{s}$. Specifically, the mean-field fluid model predicts that the distribution begins to expand much earlier than what is seen in simulation. This is due to many Lagrangian particles violating the laminar assumption leading to the incorrect assignment of force to a large proportion of the Lagrangian particles. Thus the simulation can no longer be described by our laminar model.

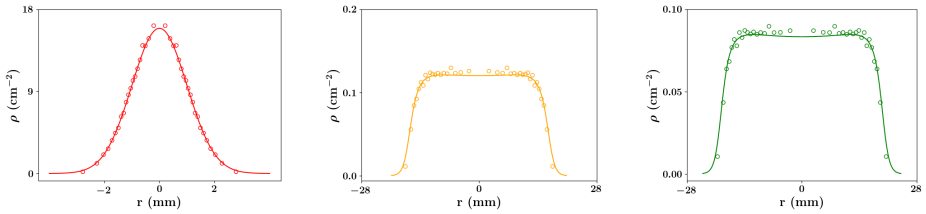

(a) initial (b) 60 ns (c) 70 ns

Fig. 4. Similar to Fig. 3 but with $v_0 = 50\frac{r_0}{R}\frac{km}{s}$ and at t is (a) 0, (b) 60 ns, (c) 70 ns. Solid lines are from the theory presented in this paper and circles are from the same single PIC simulation but at the different times. While a theoretical density peak can be seen to develop between (b) 60 ns and (c) 70 ns, this peak is below the random variance of the density and therefore may be argued to not be present.

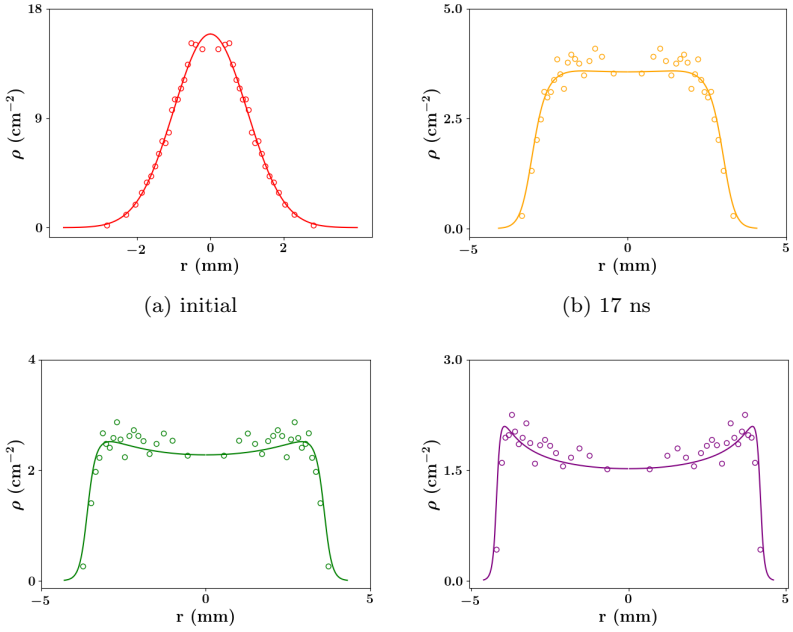

(a) initial (b) 17 ns

(c) 21 ns (d) 25 ns

Fig. 5. Similar to Fig. 3 but with $v_0 = -10\frac{r_0}{R}\frac{km}{s}$, i.e. inward instead of outward, and where t is (a) 0, (b) 17 ns, (c) 21 ns, and (d) 25 ns. Solid lines are from the theory presented in this paper and circles are from the same single PIC simulation but at the different times. Note that the density peak forms between (b) 17 ns and (c) 21 ns and is more prominent in (d) 25 ns. The emergence of this shock is slightly before what we found in the initially at rest case.[4]

To study this further, we again simulate the cylindrically-symmetric distribution but with $v_0 = C\sqrt{1 - e^{-\frac{r_0^2}{2\sigma_r^2}}}$ for $C < 0$. This velocity profile has $\frac{v_0}{v_{r2}} = \frac{C}{10^5\frac{m}{s}}$, which

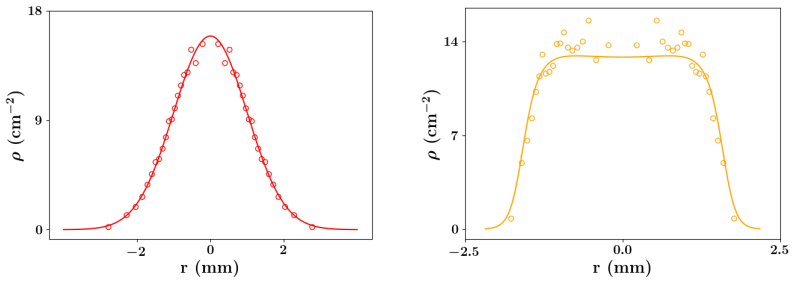

(a) initial (b) 11 ns

(c) 12 ns (d) 13 ns

Fig. 6. Similar to Fig. 5 but with $v_0 = -50\frac{r_0}{R}\frac{km}{s}$ and where t is (a) 0, (b) 11 ns, (c) 12 ns, and (d) 13 ns. Solid lines are from the theory presented in this paper and circles are from the same single PIC simulation but at the different times. Note that the density peak forms between (b) 11 ns and (c) 12 ns and is more prominent in (d) 13 ns. However, also not that the agreement between simulation and theory is not as good as previous cases.

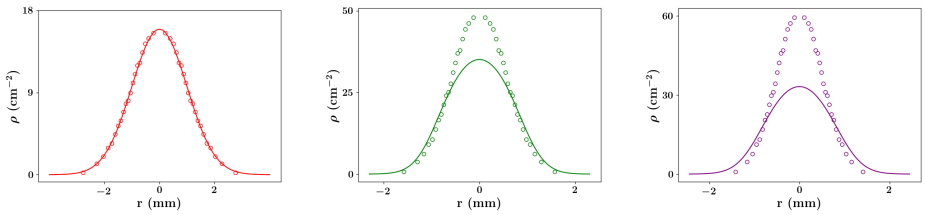

(a) initial (b) 4.4 ns (c) 5 ns

Fig. 7. Similar to Fig. 5 but with $v_0 = -100\frac{r_0}{R}\frac{km}{s}$ and where t is (a) 0, (b) 4.4 ns, and (c) 5 ns. Solid lines are from the theory presented in this paper and circles are from the same single PIC simulation but at the different times. Note that not only does the theory fail to capture the details of the simulated density, but the theoretical density is expanding between 4.4 ns but is still contracting in simulation.

is independent of r_0. This results in $r_{t2} = \alpha r_0$ where $\alpha = e^{-\frac{C^2}{10^{10}\frac{m^2}{s^2}}}$ where α is

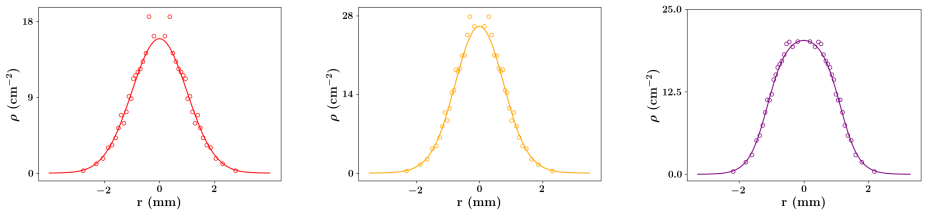

(a) initial (b) 8 ns (c) 10 ns

Fig. 8. Similar to Fig. 5 but with $v_0 = -100\frac{m}{s}\sqrt{1-e^{-\frac{r_0^2}{2\sigma_r^2}}}\,km/s$ and where t is (a) 0, (b) 6 ns, and (c) 10 ns. Solid lines are from the theory presented in this paper and circles are from the same single PIC simulation but at the different times; note the different scales on the axes for the different plots. Note that the theoretical and the simulated density evolutions are in agreement including near the focal point near (b) 6 ns as well as the portion where the distribution is again expanding as seen at (c) 10 ns.

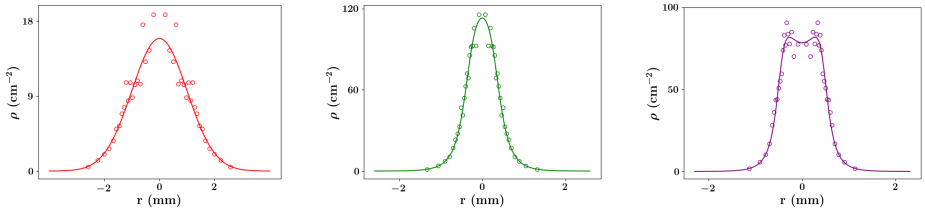

(a) initial (b) 6 ns (c) 10 ns

Fig. 9. Similar to Fig. 5 but with $v_0 = -200\frac{m}{s}\sqrt{1-e^{-\frac{r_0^2}{2\sigma_r^2}}}\,km/s$ and where t is (a) 0, (b) 6 ns, and (c) 10 ns. Solid lines are from the theory presented in this paper and circles are from the same single PIC simulation but at the different times; note the different scales on the axes for the different plots. Note that the theoretical and the simulated density evolutions are in agreement including the theory correctly predicting the location of the density peak as seen at (c) 10 ns.

independent of r_0 and $t_{t2} = \frac{2\alpha}{\omega_{02}} e^{-\frac{C^2}{10^{10}\frac{m^2}{s^2}}} F\left(\frac{C}{10^5\frac{m}{s}}\right)$; that is, the turn around points are simply scaled from the initial Gaussian, although they still occur at different times as ω_{02} is still dependent on r_0. As can be seen in Figs. 8 and 9, this distribution does appear to remain laminar through the focus as the theory is now in agreement with simulation when $v_0 > v_{r2}$; however, this comes at a cost of an early-emergence of the shock that can be seen at $10ns$ in Fig. 9c.

4. Comparison to spherically-symmetric simulations

We now demonstrate that the analysis for systems with spherical symmetry is also accurate for a wide range of initial conditions. As for the cylindrical case, we introduce a velocity term that is linear in the initial position, specifically it has the form

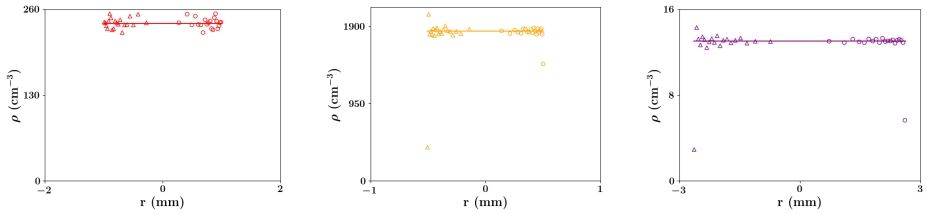

(a) initial (b) 7.5 ns (c) 30 ns

Fig. 10. The evolution of spherically symmetric 2×10^4 uniformly distributed electron in a $R = 1$ mm radius with initial velocity assigned by $v_0 = -100 \frac{r_0}{R} \frac{km}{s}$, where r_0 represent the radial position of the particle, at t is is (a) 0, (b) 7.5 ns and (c) 30 ns. Solid lines are from the theory presented in this paper and circles on the right of $r = 0$ and triangles left of $r = 0$ are from the same single PIC simulation and N-particle simulation, respectively, but at different times. Note the very different scales on the axes for the two plots, and notice that the mean-field fluid model again captures the evolution of the bunch for this case with the exception of the very edge of the N-particle simulation even through the focal point near (b) 7.5 ns.

$v_0(r_0) = C \frac{r_0}{R}$ where C is a simulation dependent constant and R is the initial radius of the uniform distribution. For our demonstration, we chose $Q_{tot,3} = 2 \times 10^4 e$ and $R = 1mm$, and this again corresponds to a $v_{r3} \approx 10^5 \frac{m}{s} \frac{r_0}{R}$. We used the electrostatic Poisson solver in warp[19] as well as leapfrog algorithm with the FMM algorithm[20] to determine the force on the particles in our own fortran code. Fig. 10 shows the results for the value of C corresponding to inward focussing and roughly the size of v_{r3}, $-10^5 \frac{m}{s}$. Notice the excellent agreement between theory and simulation in all cases thus validating the use of the spherically-symmetric formulation.

5. Conclusions

Here, we presented a mean-field fluid model for the evolution of cylindrically and spherically symmetric charged bunches with arbitrary initial distribution and initial velocity that can be written as a function of the radial coordinate. We demonstrated that this model predicts the density evolution of the initially uniform bunch when the initial velocity distribution is linear under both spherical and cylindrical geometries. In the cylindrical geometry, we showed that the shock that arises in the cold Gaussian distribution slightly prior to the onset of the non-laminar regime can be suppressed by introducing a initial radially-outward velocity distribution whose linear proportionality constant is of the order or greater than $\sqrt{\frac{qQ_{tot,2}}{\pi m \epsilon_0}}$. However, when an analogous negative linear velocity distribution is introduced, the model disagrees with simulations as the initial velocity results in a rapid violation of the laminar assumption. Nonetheless, by adjusting the functional form of the initially velocity distribution from $\frac{r_0}{R}$ to $\sqrt{1 - e^{-\frac{r_0^2}{2\sigma_r^2}}}$, we demonstrated that the model can predict the evolution of the initially Gaussian distribution through the focus including the emergence of a shock. This suggests that the laminar assumption for the Gaussian

distribution is not violated by this functional form of the velocity distribution, at least for the duration of time we simulated.

The velocity scales derived in this paper, v_{r2} and v_{r3}, present the means to qualitatively understand when the laminar assumption can be made. For the uniform distribution, $v_{rd} \propto \frac{r_0}{R}$. Thus linear momentum kicks should result in the evolution of the distribution remaining laminar even when the kick is inward; however, if the inward kick has a functional form where the slope of the function is beyond linear, say $v_0 \propto \frac{r_0^2}{R^2}$, outer Lagrangian particle trajectories will cross the trajectories of inner Lagrangian particles and the laminar assumption will be violated. Analogously for the Gaussian distribution, $v_{rd} \propto \sqrt{1-e^{-\frac{r_0^2}{2\sigma_r^2}}}$, so it is the slope of this function that matters; that is, the linear kick, where $v_{rd} \propto \frac{r_0}{R}$, has slope beyond $\sqrt{1-e^{-\frac{r_0^2}{2\sigma_r^2}}}$ resulting in violation of the laminar assumption. On the other hand, using $\sqrt{1-e^{-\frac{r_0^2}{2\sigma_r^2}}}$ as the functional form of the velocity distribution, the density evolution of the laminar theory and the simulation remain in agreement even through focal points as seen in this work. This brings us to the conclusion that such non-linear focussing results in the beam retaining laminar flow through the focal point until the laminar assumption is later violated by the shock dynamics as we have discussed in our previous work.[4]

In other words, the model we have presented here provides an accurate description of the density evolution of a beam as it expands and focusses as long as the beam dynamics exhibits laminar flow. The model also lends important insight into the parameters that drive the beam into non-laminar conditions; specifically shortly after the emergence of a shock and when the focussing kick has a functional form beyond what is needed for the specific distribution. Of course, our theoretical initial distributions arguably still have zero emittance as v_0 is exactly specified by r_0. The arguably comes from the fact that this initial velocity need not be linear in r_0, and hence the rms normalized emittance measure need not be zero; however, the initial local momentum width at each x is zero. On the other hand, the initial spatial distribution in the simulations was sampled, and this process does make the beam effectively warm as the sampling introduces disorder induced heating into the distribution.[21] Despite the beam being having non-zero emittance after initialization, though, the model correctly predicts the focussing behavior of both the initially uniform and Gaussian distributions provided that the laminar criteria are met. Presumably if the emittance is high enough, the model will fail, and an exploration of this condition is reserved for future work; as is extending the analysis presented here to the relativistic regime. The question of whether it is better to remain within this laminar regime or to allow mixing is also worth investigating as we now understand many of the conditions to prevent Lagrangian particle mixing.

6. Acknowledgements

This work was supported by NSF Grant numbers RC1803719 and RC108666. Useful discussions with Steve Lund and Chong-Yu Ruan are gratefully acknowledged.

Appendix A. First order derivatives

In this appendix, we derivatives the expressions Eqs (21) - (24). We start this by taking the derivative, $' \equiv \frac{d}{dr_0}$, of all parameters discussed in the main text. Starting with the cumulative probabilities we have

$$P'_{02} = 2\pi r_0 \rho_{02} \tag{A.1}$$

$$P'_{03} = 4\pi r_0^2 \rho_{03} \tag{A.2}$$

Now the derivatives of the average probability-like distribution is

$$\bar{\rho}'_{02} = \frac{2\bar{\rho}_{02}}{r_0}\left(\frac{\rho_{02}}{\bar{\rho}_{02}} - 1\right) \tag{A.3}$$

$$\bar{\rho}'_{03} = \frac{3\bar{\rho}_{03}}{r_0}\left(\frac{\rho_{03}}{\bar{\rho}_{03}} - 1\right) \tag{A.4}$$

Next, the derivative of the initial energy term

$$\mathcal{E}'_0 = m v_0 v'_0 \tag{A.5}$$

and then the derivatives of the energy scale terms

$$\mathcal{E}'_{r2} = \frac{qQ_{tot,2}}{\epsilon_0} r_0 \rho_{02} \tag{A.6}$$

$$\mathcal{E}'_{r3} = \frac{qQ_{tot,3}}{\epsilon_0} r_0 \left(\rho_{03} - \frac{1}{3}\bar{\rho}_{03}\right) \tag{A.7}$$

This can be used to show

$$v'_{r2} = \frac{v_{r2}}{r_0}\frac{\rho_{02}}{\bar{\rho}_{02}} \tag{A.8}$$

$$v'_{r3} = \frac{1}{2}\frac{v_{r3}}{r_0}\left(3\frac{\rho_{03}}{\bar{\rho}_{03}} - 1\right) \tag{A.9}$$

For the cylindrical turn around point, we can write Eq. (7) as

$$r_{t2} = r_0 e^{-\frac{\mathcal{E}_0}{\mathcal{E}_{r2}}}$$

it follows

$$\begin{aligned} r'_{t2} &= \frac{r_{t2}}{r_0} - r_{t2}\left(\frac{\mathcal{E}'_0}{\mathcal{E}_{r2}} - \frac{\mathcal{E}_0 \mathcal{E}'_{r2}}{\mathcal{E}_{r2}^2}\right) \\ &= \frac{r_{t2}}{r_0}\left(1 - 2\frac{v_0}{v_{r2}}\frac{r_0 v'_0}{v_{r2}} + 2\frac{v_0^2}{v_{r2}^2}\frac{\rho_{02}}{\bar{\rho}_{02}}\right) \end{aligned} \tag{A.10}$$

For the spherical turn around point, we can write Eq. (8) as

$$r_{t3} = \frac{r_0}{1 + \frac{\mathcal{E}_0}{\mathcal{E}_{r3}}} \tag{A.11}$$

it follows

$$\begin{aligned} r'_{t3} &= \frac{r_{t3}}{r_0} - \frac{r_{t3}}{1+\frac{\mathcal{E}_0}{\mathcal{E}_{r3}}}\left(\frac{\mathcal{E}'_0}{\mathcal{E}_{r3}} - \frac{\mathcal{E}_0\mathcal{E}'_{r3}}{\mathcal{E}^2_{r3}}\right) \\ &= \frac{r^2_{t3}}{r^2_0}\left(1 - 2\frac{v_0}{v_{r3}}\frac{r_0 v'_0}{v_{r3}} + 3\frac{v^2_0}{v^2_{r3}}\frac{\rho_{03}}{\bar{\rho}_{03}}\right) \end{aligned} \tag{A.12}$$

Next, the derivative of the average probability-like densities at the turn-around point are

$$\bar{\rho}'_{t2} = \frac{2\bar{\rho}_{t2}}{r_{t2}}\left(\frac{r_0}{r_{t2}}\frac{\rho_{02}}{\bar{\rho}_{t2}} - r'_{t2}\right) \tag{A.13}$$

$$\bar{\rho}'_{t3} = \frac{3\bar{\rho}_{t3}}{r_{t3}}\left(\frac{r^2_0}{r^2_{t3}}\frac{\rho_{03}}{\bar{\rho}_{t3}} - r'_{t3}\right) \tag{A.14}$$

The derivative of the associated plasma frequencies are

$$\begin{aligned} \omega'_{t2} &= \frac{\omega_{t2}}{2\bar{\rho}_{t2}}\bar{\rho}'_{t2} \\ &= \frac{\omega_{t2}}{r_0}\left(\frac{\rho_{02}}{\bar{\rho}_{02}} - \frac{r_0}{r_{t2}}r'_{t2}\right) \end{aligned} \tag{A.15}$$

$$\begin{aligned} \omega'_{t3} &= \frac{\omega_{t3}}{2\bar{\rho}_{t3}}\bar{\rho}'_{t3} \\ &= \frac{3}{2}\frac{\omega_{t3}}{r_0}\left(\frac{\rho_{03}}{\bar{\rho}_{03}} - \frac{r_0}{r_{t3}}r'_{t3}\right) \end{aligned} \tag{A.16}$$

Finally, the derivative of the transit time to the turn around point in the cylindrical case is

$$\begin{aligned} t'_{t2} &= -\frac{t_{t2}}{\omega_{t2}}\omega'_{t2} + t_{t2}\frac{1}{r_0}\left(2\frac{v_0}{v_{r2}}\frac{r_0 v'_0}{v_{r2}} - 2\frac{v^2_0}{v^2_{r2}}\frac{\rho_{02}}{\bar{\rho}_{02}}\right) \\ &\quad + \frac{2}{\omega_{t2}}e^{\frac{v^2_0}{v^2_{r2}}}\left(1 - 2\frac{v_0}{v_{r2}}F\left(\frac{v_0}{v_{r2}}\right)\right)\left(\frac{v'_0}{v_{r2}} - \frac{v_0 v'_{r2}}{v^2_{r2}}\right) \\ &= -\frac{t_{t2}}{\omega_{t2}}\omega'_{t2} + \frac{2}{\omega_{t2}}\frac{v_0}{v_{r2}}e^{\frac{v^2_0}{v^2_{r2}}}\frac{1}{r_0}\left(\frac{r_0 v'_0}{v_0} - \frac{\rho_{02}}{\bar{\rho}_{02}}\right) \end{aligned} \tag{A.17}$$

and for spherical symmetry

$$
\begin{aligned}
t'_{t3} &= -\frac{t_{t3}}{\omega_{t3}}\omega'_{t3} + \frac{1}{\omega_{t3}} \\
&\quad \times \left(-\frac{1+\frac{v_{r3}^2}{v_0^2}}{\frac{v_{r3}^2}{v_0^2}} \frac{1}{2\left(1+\frac{v_{r3}^2}{v_0^2}\right)^{3/2}} 2\frac{v_{r3}}{v_0}\left(\frac{v'_{r3}}{v_0} - \frac{v_{r3}v'_0}{v_0^2}\right) \right. \\
&\quad \left. + \left(\frac{v'_0}{v_{r3}} - \frac{v_0 v'_{r3}}{v_{r3}^2}\right)\left(\sqrt{1+\frac{v_0^2}{v_{r3}^2}} + \frac{v_0^2}{v_{r3}^2}\frac{1}{\sqrt{1+\frac{v_0^2}{v_{r3}^2}}}\right)\right) \\
&= -\frac{t_{t3}}{\omega_{t3}}\omega'_{t3} + \frac{1}{\omega_{t3}}\frac{1}{\sqrt{1+\frac{v_0^2}{v_{r3}^2}}}\left(-\frac{v_0}{v_{r3}}\left(\frac{v'_{r3}}{v_{r3}} - \frac{v'_0}{v_0}\right)\right. \\
&\quad \left. + \frac{v_0}{v_{r3}}\left(\frac{v'_0}{v_0} - \frac{v'_{r3}}{v_{r3}}\right)\left(1+2\frac{v_0^2}{v_{r3}^2}\right)\right) \\
&= -\frac{t_{t3}}{\omega_{t3}}\omega'_{t3} + \frac{1}{\omega_{t3}}\frac{v_0}{v_{r3}}\sqrt{1+\frac{v_0^2}{v_{r3}^2}}\frac{1}{r_0}\left(1+2\frac{r_0 v'_0}{v_0} - 3\frac{\rho_{03}}{\bar{\rho}_{03}}\right)
\end{aligned}
\tag{A.18}
$$

References

1. O. J. Luiten, S. B. vanderGeer, M. J. deLoos, F. B. Kiewiet, and M. J. vanderWiel, "How to realize uniform three-dimensional ellipsoidal electron bunches," *Physical review letters*, vol. 93, no. 9, p. 094802, 2004.
2. C. C. Lin, L. Mestel, and F. H. Shu, "The gravitational collapse of a uniform spheroid," *The Astrophysical Journal*, vol. 142, pp. 1431–1446, 1965.
3. P. Musumeci, J. T. Moody, R. J. England, J. B. Rosenzweig, and T. Tran, "Experimental generation and characterization of a uniformly filled ellipsoidal electron-beam distributions," *Physical review letters*, vol. 100, no. 24, p. 244801, 2008.
4. B. Zerbe, X. Xiang, C.-Y. Ruan, S. Lund, and P. Duxbury, "Dynamical bunching and density peaks in expanding coulomb clouds," *Physical Review Accelerators and Beams*, vol. 21, no. 6, p. 064201, 2018.
5. O. Anderson, "Internal dynamics and emittance growth in space charge dominated beams," *Part. Accel.*, vol. 21, pp. 197–226, 1987.
6. L. Serafini and J. B. Rosenzweig, "Envelope analysis of intense relativistic quasilaminar beams in rf photoinjectors: ma theory of emittance compensation," *Physical Review E*, vol. 55, no. 6, p. 7565, 1997.
7. J. Rosenzweig, A. Cook, R. England, M. Dunning, S. Anderson, and M. Ferrario, "Emittance compensation with dynamically optimized photoelectron beam profiles," *Nuclear Instruments and Methods in Physics Research Section A: Accelerators, Spectrometers, Detectors and Associated Equipment*, vol. 557, no. 1, pp. 87–93, 2006.
8. B. J. Siwick, J. R. Dwyer, R. E. Jordan, and R. J. Dwayne Miller, "Ultrafast electron optics: Propogation dynamics of femtosecond electron packets," *Journal of Applied Physics*, vol. 92, no. 3, pp. 1643–1648, 2002.
9. B.-L. Qian and H. E. Elsayed-Ali, "Electron pulse broadening due to space charge effects in a photoelectron gun for electron diffraction and streak camera systems," *Journal of Applied Physics*, vol. 91, no. 1, pp. 462–468, 2002.

10. B. W. Reed, "Femtosecond electron pulse propagation for ultrafast electron diffraction," *Journal of Applied Physics*, vol. 100, no. 3, pp. 034 916–034 931, 2006.
11. M. Grech, R. Nuter, A. Mikaberidze, P. Di Cintio, L. Gremillet, E. Lefebvre, U. Saalmann, J. M. Rost, and S. Skupin, "Coulomb explosion of uniformly charged spheroids," *Physical Review E*, vol. 84, no. 5, pp. 056 404–056 414, 2011.
12. A. E. Kaplan, B. Y. Dubetsky, and P. L. Shkolnikov, "Shock shells in coulomb explosions of nanoclusters," *Physical review letters*, vol. 91, no. 14, p. 143401, 2003.
13. V. Kovalev and V. Y. Bychenkov, "Kinetic description of the coulomb explosion of a spherically symmetric cluster," *Journal of Experimental and Theoretical Physics*, vol. 101, no. 2, pp. 212–223, 2005.
14. I. Last, I. Schek, and J. Jortner, "Energetics and dynamics of coulomb explosion of highly charged clusters," *The Journal of chemical physics*, vol. 107, no. 17, pp. 6685–6692, 1997.
15. D. Murphy, R. Speirs, D. Sheludko, C. Putkunz, A. McCulloch, B. Sparkes, and R. Scholten, "Detailed observation of space–charge dynamics using ultracold ion bunches," *Nature communications*, vol. 5, p. 4489, 2014.
16. V. P. Degtyareva, M. A. Monastyrsky, M. Y. Schelev, and V. A. Tarasov, "Computer studies on dynamics of ultrashort electron packets in streak tubes and diffractometers," *Optical Engineering*, vol. 37, no. 8, pp. 2227–2232, 1998.
17. V. Kovalev, K. Popov, V. Y. Bychenkov, and W. Rozmus, "Laser triggered coulomb explosion of nanoscale symmetric targets," *Physics of plasmas*, vol. 14, no. 5, p. 053103, 2007.
18. T. P. Wangler, *RF Linear accelerators*. John Wiley & Sons, 2008.
19. A. Friedman, R. H. Cohen, D. P. Grote, S. M. Lund, W. M. Sharp, J.-L. Vay, I. Haber, and R. A. Kishek, "Computational methods in the warp code framework for kinetic simulations of particle beams and plasmas," *IEEE Transactions on Plasma Science*, vol. 42, no. 5, pp. 1321–1334, 2014.
20. Z. Gimbutas and L. Greengard, "Computational software: Simple fmm libraries for electrostatics, slow viscous flow, and frequency-domain wave propagation," *Communications in Computational Physics*, vol. 18, no. 2, pp. 516–528, 2015.
21. J. Maxson, I. Bazarov, W. Wan, H. Padmore, and C. Coleman-Smith, "Fundamental photoemission brightness limit from disorder induced heating," *New Journal of Physics*, vol. 15, no. 10, p. 103024, 2013.